

Chiral Magnets

Trinuclear Complexes Derived from *R/S* Schiff Bases – Chiral Single-Molecule Magnets

Albert Escuer^[a], Julia Mayans,^[a] Merce Font-Bardia,^[b] Lorenzo Di Bari,^[c] and Marcin Górecki^[c]

Abstract: The employment of enantiomerically pure Schiff bases in manganese chemistry is revealed to be an excellent method to obtain chiral single-molecule magnets and has allowed the characterization of several pairs of enantiomers, for

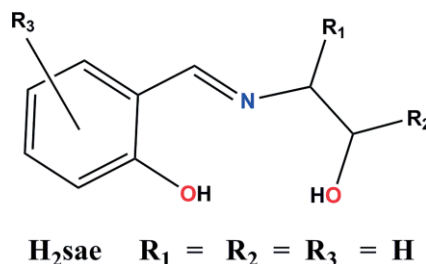
which the magnetic properties were investigated. The reported systems consist of Mn^{III}–Mn^{II}–Mn^{III} linear trimers or Mn^{III}₃ cations in a triangular arrangement including the first example of a μ₃-Cl bridge in an isolated manganese triangle.

Introduction

Research on coordination clusters of paramagnetic 3d or 4f cations has been key in the search for single-molecule magnets (SMMs) or single-ion magnets (SIMs)^[1] and more recently for their catalytic,^[2] bioinorganic,^[3] and optical^[4] properties. The exploration of molecular systems that crystallize in chiral space groups is still an emerging field, and the possible chiral organization of magnetic moments can produce quite exotic properties such as the predicted skyrmions^[5] or chiral solitons.^[6] The spontaneous crystallization of nonchiral components in chiral groups or the resolution of racemic mixtures are unusual^[7] or experimentally difficult; therefore, syntheses with enantiomerically pure chiral ligands have become the optimal method to reach systems of this kind.^[8]

The condensation of salicylaldehyde and 1,2-aminoethanol yields the Schiff base 2-[(2-hydroxyethyl)iminomethyl]phenol (H₂sae, Scheme 1). H₂sae is a popular ligand and has been employed widely in transition-metal and lanthanide coordination chemistry (around 110 entries in the CCDC) owing to its good chelating properties and its ability to generate polynuclear systems through the potentially bridging O-phenolate and O-alkoxido donors.

The chemistry of manganese with nonchiral Schiff bases such as H₂sae or their substituted analogs has been partially explored in the recent past to yield a variety of systems such



Scheme 1. General structural formula for the H₂sae ligand and its substituted derivatives. The variation of the R₁ and R₂ groups allows the synthesis of chiral ligands.

as neutral mononuclear Mn^{IV} complexes,^[9] one Mn^{III} 1D system,^[10] and several homometallic Mn^{II}Mn^{III}₂,^[11] Mn^{III}₄ (ring),^[12] Mn^{III}₄ (butterfly),^[12c,13] Mn^{III}₆, Mn^{II}Mn^{III}₄, and Mn^{III}₈ clusters^[13,14] as well as heterometallic^[15] Cu^{II}₃Mn^{III} and Ni^{II}₂Mn^{III}₂ clusters. Among them, the magnetic properties of the tetranuclear cyclic systems with general formula [Mn^{III}₄X₄L₄] (X = Cl, Br) have been the most interesting, as they display ferromagnetic interactions and SMM responses.^[12b]

The substitution on the aromatic ring or the C atoms of the ethyl fragment can increase the number of Schiff bases enormously, and chirality can be induced if the substitution occurs at the 1- or 2-position of the hydroxyethyl group (Scheme 1).

Following our work in this field, we have explored the reactivity in manganese chemistry of the enantiomerically pure ligands (*R*)- and (*S*)-2-[(2-hydroxy-1-phenylethyl)iminomethyl]phenol] (H₂L1) and (*R*)- and (*S*)-2-[(3-hydroxy-1-phenylpropyl)iminomethyl]phenol] (H₂L2, Scheme 2).

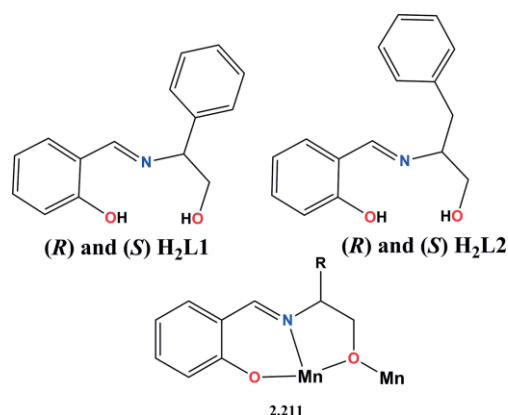
The reactions of these ligands with different manganese salts under appropriate reaction conditions allowed the characterization of the first polynuclear derivatives of H₂L1/H₂L2 consisting of three pairs of trinuclear chiral clusters with formulas [Mn₃(L1)₂(PhCOO)₄(MeOH)] [(*R*)-1·MeOH and (*S*)-1·MeOH], [Mn₃(L2)₂(PhCOO)₄] [(*R*)-2·5H₂O and (*S*)-2·2MeCN·MeOH·1.5H₂O], and (Phgly)[Mn₃(L1)₃(μ₃-Cl)(Cl)₃] [(*R*)-3·0.5MeCN·0.25MeOH·0.5H₂O and (*S*)-3·0.5MeCN·0.5H₂O; Phgly = phenyl-

[a] Departament de Química Inorgànica i Orgànica, Secció Inorgànica and Institute of Nanoscience (IN²UB) and Nanotechnology, Universitat de Barcelona, Av. Diagonal 645, 08028 Barcelona, Spain
E-mail: albert.escuer@ub.edu
<http://www.ub.edu/inorgani/reerca/MagMol/magmol.htm>

[b] Departament de Mineralogia, Cristallografia i Dipòsits Minerals and Unitat de Difracció de R-X, Centre Científic i Tecnològic de la Universitat de Barcelona (CCITUB), Universitat de Barcelona, Solé i Sabarís 1–3 08028 Barcelona, Spain

[c] Dipartimento di Chimica e Chimica Industriale, Università di Pisa, Via Moruzzi 13, I-56124 Pisa, Italy

Supporting information and ORCID(s) from the author(s) for this article are available on the WWW under <http://dx.doi.org/10.1002/ejic.201601138>.



Scheme 2. Structures of H_2L1 and H_2L2 ligands (top) and their crystallographically established coordination mode in complexes **1–3** (bottom).

glycinate]. Complexes **1** and **2** have linear $\{Mn^II Mn^{III}_2(\mu-O)_2(RCOO)_4\}$ cores, whereas **3** has a triangular arrangement with an unprecedented $\{Mn^{III}_3(RO)_3(\mu_3-Cl)\}$ linkage and SMM response.

Results and Discussion

Structural Descriptions

Each pair of enantiomers is very similar; therefore, a common structural description is provided for the corresponding *R* enantiomer. The oxidation states of the manganese atoms have been assigned on the basis of structural considerations and bond valence sum (BVS) calculations. The bond parameters for each pair of enantiomers are summarized in Table S2 for (*R*)-**1** and (*S*)-**1**, Table S3 for (*R*)-**2** and (*S*)-**2**, and Table S4 for (*R*)-**3**. Some significant bond parameters for (*S*)-**3** are also provided in Table S4.

$[Mn_3(L1)_2(PhCOO)_4(MeOH)] \cdot MeOH$ [(*R*)-**1**-MeOH and (*S*)-**1**-MeOH]

Compounds (*R*)-**1** and (*S*)-**1** can be described as linear trinuclear $Mn^{III}_2Mn^{II}$ systems, in which the Mn^{II} cation is in the central position and linked to both Mn^{III} cations by two *syn-syn* carboxylate bridges and one alkoxido bridge. A view of the complex is shown in Figure 1, and the main bond parameters are summarized in Table S2. The trinuclear system is almost linear [the $Mn(1) \cdots Mn(2) \cdots Mn(3)$ angle is close to 178°]. The divalent $Mn(2)$ cation shows an MnO_6 octahedral environment, whereas the trivalent $Mn(1)$ cation exhibits an octahedral MnO_5N coordination with the elongated Jahn–Teller axis directed toward the $O(5)$ -carboxylato atom and the coordinated methanol molecule, and $Mn(3)$ shows a square-pyramidal MnO_4N environment with the apical position occupied by the $O(8)$ donor from one of the carboxylate groups.

The angle between the main $O10-O11-O12-N2$ and $O1-O2-O3-N1$ planes is 6.2° ; thus, the easy axes of the two Mn^{III} cations, defined by the $Mn3-O8$ and $O5-Mn1-O1w$ directions, are approximately parallel.

The crystallization methanol molecule establish two H bonds with the coordinated methanol molecule and the $O(11)$ alkox-

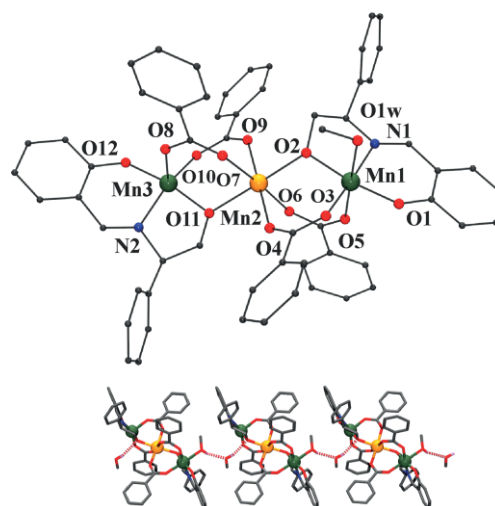


Figure 1. Top: partially labeled plot of **1** [common labels for (*R*)-**1** and (*S*)-**1**]. Bottom: 1D arrangement of trinuclear units linked by intermolecular H bonds (red dashed bonds). H atoms omitted for clarity. Color key: Mn^{II} orange, Mn^{III} dark green, O red, N navy, C grey.

ido atom of the neighboring clusters to afford a 1D arrangement of trimers. The $O(1w) \cdots O(2w)$ and $O(1w) \cdots O(11)$ distances are 2.764 and 2.984 Å, respectively.

$[Mn_3(L2)_2(PhCOO)_4(MeOH)] \cdot Solvent$ [(*R*)-**2**- $5H_2O$, (*S*)-**2**- $2MeCN \cdot MeOH \cdot 1.5H_2O$]

The trinuclear compounds (*R*)-**2** and (*S*)-**2** show the same general formulas and connectivities as (*R*)-**1** and (*S*)-**1** but significant differences in the manganese coordination spheres and the arrangement of the ligands. A view of the complex is shown in Figure 2, and the main bond parameters are summarized in Table S3.

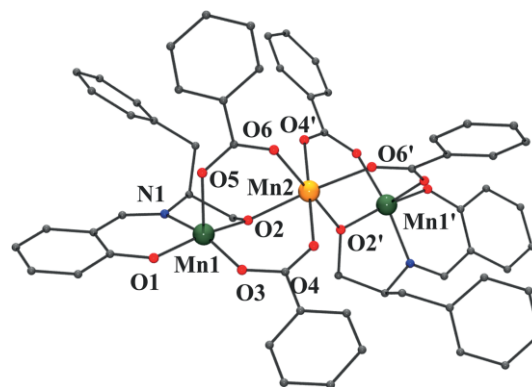


Figure 2. Partially labeled plot of **2** [common labels for (*R*)-**2** and (*S*)-**2**].

For **2**, the two moieties of the complex are related by one C_2 axis, which results in a more symmetrical molecule than **1**. In this case, the trinuclear complex has a $Mn(1) \cdots Mn(2) \cdots Mn(1')$ angle of 135° , and the carboxylate ligands are placed on the same side of the mean trimer plane. $Mn(1)$ and symmetry-related $Mn(1')$ are pentacoordinate with MnO_4N square-pyramidal environments, whereas the divalent $Mn(1)$ cation is octahedrally coordinated.

The angle determined by the mean planes that define the base of the square pyramids (O1–O2–O3–N1 and the symmetry-related counterpart) is 44.6°; consequently, the angle between the easy axes of the Mn^{III} cations is also close to 45°.

**(Phgly)[Mn₃(L1)₃(μ₃-Cl)(Cl)₃]-0.5MeCN-0.5H₂O-0.25MeOH
[(*R*)-**3**-0.5MeCN-0.5H₂O-0.25MeOH]**

Complex (*R*)-**3** can be described as a triangular arrangement of three Mn^{III} ions linked by *O*-alkoxido donors and one μ₃-Cl bridge. A view of the complex is shown in Figure 3, and the main bond parameters are summarized in Table S4. The Mn^{III} cations are octahedrally coordinated with a MnCl₂O₃N environment. One L1²⁻ Schiff base is coordinated to each manganese atom through their three donor atoms and acts as an *O*-alkoxido bridge to the neighboring cation. The coordination sphere is completed by two chlorido ligands in *trans* positions, one of which acts as a μ₃-Cl bridge. The easy axis corresponding to the elongated axis of the octahedron follows the Cl–Mn–Cl direction, and the mean O₃N planes of the Mn^{III} cations are tilted by ca. 58° as consequence of this arrangement.

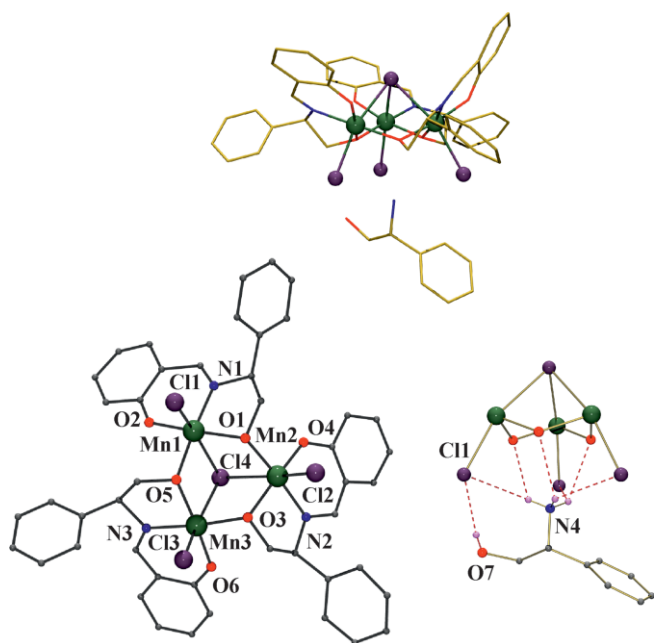


Figure 3. Left: partially labeled plot of (*R*)-**3**. The partial resolution of the structure confirmed the same core for (*S*)-**3**. Right: H bonds involving the trimeric complex and the protonated Phgly⁺ cation. Color scheme: Mn^{III} dark green, O red, N navy, Cl violet, C grey, H pink.

The trinuclear entity is monoanionic, and charge balance is provided by one protonated phenylglycinate cation [(*R*)- or (*S*)-Phgly⁺ for (*R*)-**3** or (*S*)-**3**, respectively], which is linked to the three terminal chlorido ligands and the *O*-alkoxido atoms through six H bonds promoted by the RNH₃⁺ fragment. No relevant intermolecular interactions were found.

It should be emphasized that complexes **3** are the only examples of discrete triangular Mn^{III} systems with one μ₃-Cl bridge. This kind of bridge has been reported previously for cubanes with {Mn₄O₃Cl} cores in which one corner^[16] is occupied by the chlorido ligand or as a fragment of a larger cluster.

Comments on the Syntheses

The reactions of H₂L1 and H₂L2 with manganese carboxylates yielded the trinuclear Mn^{II}Mn^{III}₂ systems **1** and **2**, which show the very stable {Mn^{II}Mn^{III}₂(μ-O)₂(RCOO)₄} core. This kind of complex is well known for most transition-metal cations; for manganese, they often form from the reactions of manganese carboxylates with bi- or tridentate ligands. Notably, the cores of **1** and **2** are closely related, and the main difference lies in the rotation of one of the moieties by ca. 60° (Figure 4).

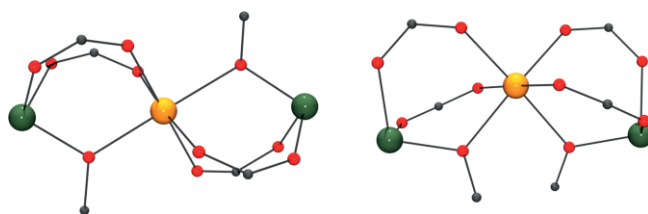
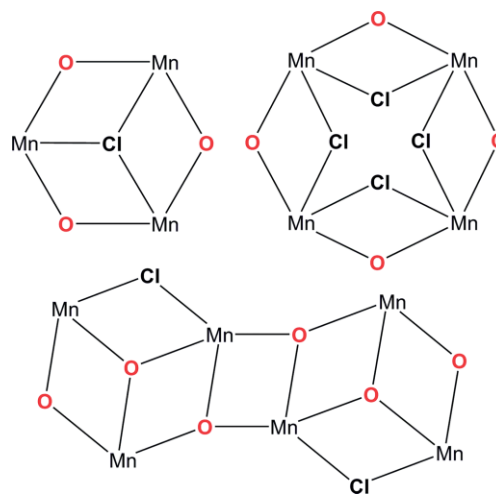


Figure 4. Cores of **1** (left) and **2** (right).

More interesting are the reactions of H₂L (H₂sae or substituted derivatives) with MnCl₂ (Scheme 3). Tetranuclear rings with four μ-O and four μ-Cl bridges formed through the reactions of MnCl₂ and the Schiff base (1:1) in ethanol followed by recrystallization in acetonitrile/diethyl ether.^[12a,12b]



Scheme 3. Tri-, tetra-, and hexanuclear cores of the clusters reported previously through the reactions of MnCl₂ and H₂sae (or substituted derivatives). All oxygen bridges are provided by the *O*-alkoxido atoms of the sae²⁻ ligands.

In that case, the deprotonation of the ligand was induced by the trivalent manganese centers because no base was added. The same core was also formed through the reaction of MnCl₂, the Schiff base, and sodium benzoate (in a 4:2:1 ratio) in hot acetonitrile.^[12c] In contrast, a hexanuclear Mn^{II}₂Mn^{III}₄ core was obtained through the reaction of MnCl₂, the Schiff base, and triethylamine (in a 1:1:2 ratio) in methanol.^[14] In our case, (*R*)-**3** and (*S*)-**3** were obtained through the reaction of MnCl₂, the chiral Schiff base, and sodium benzoate (in a 1:1:1 ratio) in acetonitrile under reflux.

The deprotonation of the H₂L ligands occurs in neutral and basic media, and a comparison of the reaction conditions suggests that it is hard to extract any justification for the different

nuclearities. The most probable factor that allows the formation of triangular systems **3** is the partial breaking of the ligand during the heating of the reaction mixture under reflux to regenerate the Phgly⁺ cation, which helps to stabilize the structure. The only conclusion is that these systems are very sensitive to small changes in the synthetic procedures, and a rich cluster chemistry can be advanced by the systematic study of reactions with the variation of the strength of the basic medium, the H₂sae substituents, or the solvent.

Electronic Circular Dichroism Spectra

Electronic circular dichroism (ECD) spectroscopy represents a crucial tool in structural studies of chiral coordination compounds.^[17] Generally, the chirality in such systems may be induced by a chiral ligand, by the intrinsic chirality of metal coordination, or both. The ECD and absorption (UV/Vis) spectra of the complexes in solution (CH₃CN) and in the solid state (KCl pellets) were measured. The solid-state ECD spectra of both enantiomers of **1–3** (Figure 5) and those recorded in acetonitrile

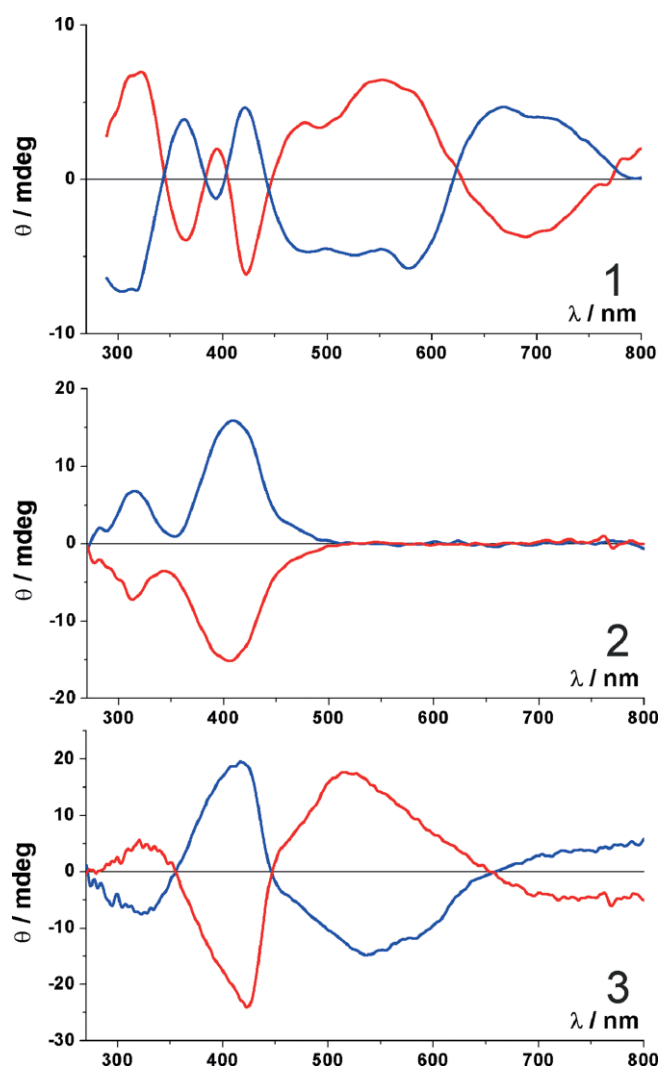


Figure 5. Solid-state ECD spectra for the pairs of enantiomers of **1–3** (red lines, *S* enantiomers; blue lines, *R* enantiomers).

solution for both enantiomers of **2** and **3** are perfect mirror images of each other (see Supporting Information, Figures S1 and S2); this confirms the enantiomeric purity and also artefact-free character of the solid-state spectra. The solid-state ECD spectra again showed some regularities. For (*S*)-**1** and (*S*)-**3**, there is a common sequence of ECD bands: negative in the range $\lambda = 650\text{--}800$ nm, positive at $\lambda \approx 550$ nm, and negative at $\lambda \approx 400$ nm [also present for (*S*)-**2**]. Owing to the low solubility of **1**, the acetonitrile solution was prepared by heating for several minutes, and we noticed that the spectra for the two enantiomers were not exact mirror images (Figure S3). The sum of the two ECD spectra should give zero or, for different enantiomeric purity, a spectrum identical to that of one of the two enantiomers. This is not the case, as shown in Figure S4; therefore, some inequivalent decomposition occurs during the heating process.

All of the absorption spectra of the complexes in acetonitrile solution are fairly similar to each other (see Figures S1–S3). The spectra show a very weak band at $\lambda \approx 470$ nm (this band is not developed for **3**), a moderately intense band at $\lambda \approx 390$ nm, and two intense bands at $\lambda = 270$ and $\lambda \approx 230$ nm. Similarly to the absorption spectra, the ECD spectra display a few common features, especially in the range $\lambda = 300\text{--}800$ nm. All of the complexes with the *S* ligand configuration, that is, (*S*)-**1**, (*S*)-**2**, and (*S*)-**3**, show three negative bands: one in the range $\lambda = 500\text{--}550$ nm, the second at $\lambda \approx 400$ nm, and the third one in the range $\lambda = 300\text{--}350$ nm. Furthermore, for (*S*)-**1** and (*S*)-**3**, a weak positive broad band appears in the visible range centered at $\lambda = 675$ and 595 nm, respectively. As expected, this range is not readily detectable in the absorption spectra (in the concentration range $2.0\text{--}2.7 \times 10^{-4}$ M) as the transitions have mainly d–d character.

In summary, although the chiral complexes show very different structures, the presence of the aforementioned correlations support the hypothesis that the ECD spectrum is directed mainly by the chirality of the chelating ligands rather than the chirality of the manganese coordination sphere by itself. To obtain more evidence, we compared the solution and solid-state ECD spectra. Such comparisons will give a pronounced view into the differences between the molecular species in both states and shed more light on the origin of the transitions in such complex systems. For clarity, the comparisons were done for one enantiomer for each pair of compounds.

For (*S*)-**1**, the solid-state and solution ECD spectra show significant variations (Figure S5); in particular, the signs of two bands in the visible region at $\lambda \approx 550$ and 675 nm are opposite. This demonstrates that the solid-state ECD spectra are governed by intercrystalline interactions and the measured spectrum does not reflect the most stable conformer(s) in solution.

Time-dependent DFT (TDDFT) calculations of high-spin coordination compounds are still very demanding and were not performed because of the complexity of the system as a result of the complicated relationship between the geometry and the electronic configuration.^[18]

In contrast to the previous case, complexes **2**, which are more symmetric than **1** (as stated above), exhibits rather similar ECD spectra in both media (Figure 6). The only difference is the

relative intensity of the band $\lambda = 300$ nm, which suggests that the dominant conformation in solution is similar to that in the solid state. Furthermore, one can notice that the intensity of the ECD bands (in solution) are the highest among the studied set of Mn complexes.

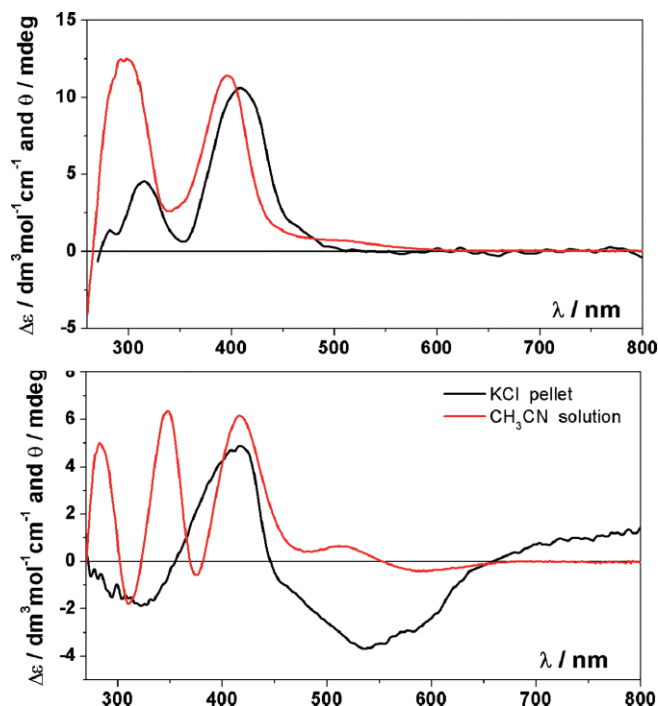


Figure 6. Comparison between the solid-state and solution ECD spectra for (R)-2 (top) and (R)-3 (bottom). Note that the solid-state spectrum of (R)-2 is divided by 1.5 and that of (R)-3 is divided by 4.

It is apparent from Figure 6 that the spectra for (R)-3 in the solid state and solution are different. This suggests that the crystal structure is not close to the predominant structure(s) in acetonitrile solution, as could be expected from the weak H-bond interactions between the triangular cluster and the phenylglycinate counteranion, which could be broken readily by interactions with the solvent.

We noticed that the studied complexes in solution and the solid state are characterized by several well-developed ECD bands. In the solution spectra, ECD bands are good indicators of the absolute configuration of the ligand, both for linear (1 and 2) and triangular (3) Mn cores. The geometry of the most prevalent conformer(s) in solution is in good agreement with the solid-state structure only for 2. Additionally, significant differences between the ECD spectra of 1 and 3 in the two media suggest a strong overlap of electronic transitions between the manganese coordination spheres and the arrangement of the ligands.

Magnetic Properties

The $\chi_M T$ versus T plots for the pairs of enantiomers of 1–3 are shown in Figure 7. The room-temperature $\chi_M T$ values for the enantiomers (R)-1 and (S)-1 are 8.62 and 8.41 $\text{cm}^3 \text{mol}^{-1} \text{K}$ re-

spectively, clearly lower than the expected value of 10.375 $\text{cm}^3 \text{mol}^{-1} \text{K}$ for two Mn^{II} and one Mn^{III} isolated cations ($g = 2.00$). On cooling, the $\chi_M T$ values decrease continuously to a plateau at 1.5 $\text{cm}^3 \text{mol}^{-1} \text{K}$ at ca. 6 K. At very low temperatures, the decrease is more pronounced, probably because of a mixing of the intermolecular coupling mediated by H bonds, the D effect induced by the Mn^{III} cations, or the weak interaction between the terminal Mn^{III} ions.

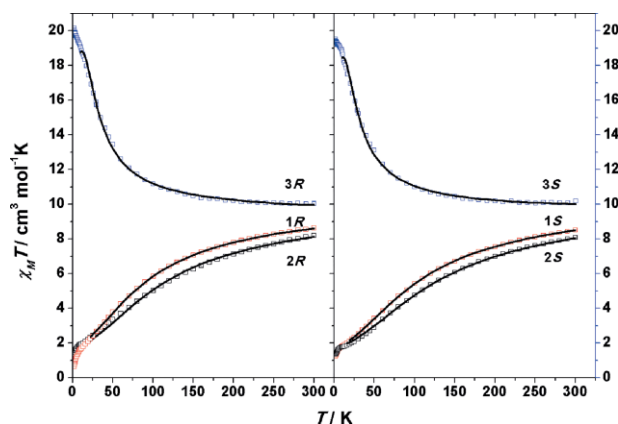


Figure 7. Plots of $\chi_M T$ versus T for (R)-1, (R)-2, (R)-3 (left) and (S)-1, (S)-2, (S)-3 (right). The solid lines are the fits of the data; see the text for the fit parameters.

To avoid overparameterization, the fit of the experimental data was performed in the 300–15 K temperature range with the conventional isotropic Hamiltonian for a linear arrangement of three $S = 2, 5/2, 2$ spins [Equation (1)]:

$$H = -2J(S_1 \cdot S_2 + S_2 \cdot S_3) \quad (1)$$

The best fit parameters were $J = -5.7 \text{ cm}^{-1}$ and $g = 2.00$ with $R = 1.53 \times 10^{-5}$ for (R)-1 and $J = -6.7 \text{ cm}^{-1}$ and $g = 2.01$ with $R = 5.17 \times 10^{-6}$ for (S)-1.

As expected from their bond parameters, complexes (R)-2 and (S)-2 exhibit similar magnetic responses to that of 1, and the room-temperature $\chi_M T$ values are 8.19 and 8.09 $\text{cm}^3 \text{mol}^{-1} \text{K}$, respectively. The fit of the experimental data was performed with the same Hamiltonian and conditions used for (R)-1 and (S)-1. The best fit parameters were $J = -7.1 \text{ cm}^{-1}$ and $g = 2.00$ with $R = 2.95 \times 10^{-4}$ for (R)-2 and $J = -8.1 \text{ cm}^{-1}$ and $g = 2.02$ with $R = 8.71 \times 10^{-5}$ for (S)-2. The magnetization under the maximum field of 5 T reached an unsaturated value close to 2.25 $\text{N}\mu_B$ for the four complexes. These values are in agreement with those reported previously for similar Schiff bases and carboxylate bridges.^[11a] The small difference between the values for each pair of enantiomers must be attributed to the different solvent molecules in the structures. Complexes (R)-3 and (S)-3 show room-temperature $\chi_M T$ values of 10.03 and 10.20 $\text{cm}^3 \text{mol}^{-1} \text{K}$, respectively, higher than the expected value of 9.00 $\text{cm}^3 \text{mol}^{-1} \text{K}$ for three isolated Mn^{III} cations. As the temperature decreases, the $\chi_M T$ products of both compounds increase to a maximum value of ca. 20 $\text{cm}^3 \text{mol}^{-1} \text{K}$, which indicates a moderate intramolecular ferromagnetic coupling.

As the Mn–Cl–Mn and Mn–O–Mn bond angles show minor differences, the system was modeled as an equilateral triangle. A first attempt to fit the experimental data isotropically in the 10–300 K temperature range was made with one J coupling constant with the Hamiltonian shown in Equation (2):

$$H = -J(S_1 \cdot S_2 + S_1 \cdot S_3 + S_2 \cdot S_3) \quad (2)$$

However, the experimental plots were not reproduced; thus, a D_{ion} term was also taken into account. An excellent match to the experimental data was obtained under these conditions with the best fit parameters $J = +1.6 \text{ cm}^{-1}$, $D_{\text{ion}} = 3.5 \text{ cm}^{-1}$, and $g = 2.03$ with $R = 9.4 \times 10^{-5}$ for (*R*)-**3** and $J = +1.5 \text{ cm}^{-1}$, $D_{\text{ion}} = 3.4 \text{ cm}^{-1}$, and $g = 2.03$ with $R = 1.3 \times 10^{-4}$ for (*S*)-**3**. From these data, an $S = 6$ ground state can be proposed.

Magnetization measurements performed at 2 K show a non-saturated value of $10.6 N\mu_{\text{B}}$ for (*R*)-**3** and 10.7 electrons for (*R*)-**3** under the maximum field of 5 T. The fits of the magnetizations for an isolated $S = 6$ ground state were satisfactory for $D = -0.42 \text{ cm}^{-1}$ and $g = 1.95$ for both compounds (Figure S6). These data confirm the $S = 6$ state and indicate a significant ground-state anisotropy.

A more precise determination of the D parameter was performed through reduced magnetization experiments (Figure 8). These measurements nicely confirmed the anisotropic character of the ground state, and excellent fits of the experimental data were obtained for $D = -0.39 \text{ cm}^{-1}$ and $g = 1.93$ for (*R*)-**3** and $D = -0.37 \text{ cm}^{-1}$ and $g = 1.92$ for (*S*)-**3**.

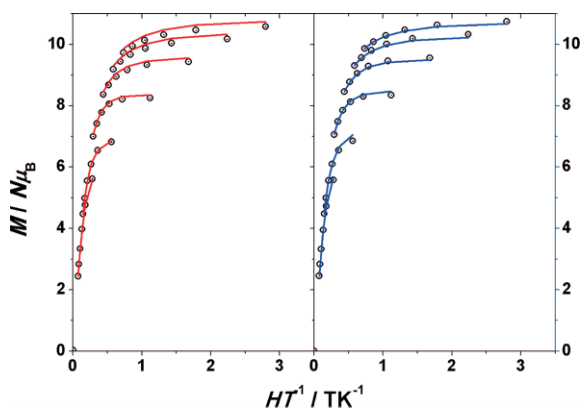


Figure 8. Reduced magnetization plots for (*R*)-**3** (left) and (*S*)-**3** (right). The solid lines show the best fits of the data.

In light of the above results, the SMM properties were explored. Alternating-current (ac) measurements at zero field only showed the tails of the out-of-phase signals, but measurements performed under a transverse magnetic field of 0.1 T broke the tunneling of the magnetization and allowed the observation of well-defined ac peaks above 2 K. The ac peaks for (*R*)-**3** and (*S*)-**3** were compared at the arbitrary frequency of 1000 Hz. They were exactly identical (Figure S7) and, thus, the complete set of measurements was performed for only one of the enantiomers [(*S*)-**3**, Figure 9]. The Arrhenius fit of the positions of the peak maxima gives a barrier for the reversal of the magnetization of $E_{\text{a}} = 17.1 \text{ cm}^{-1}$ and $\tau_0 = 9.3 \times 10^{-9}$. The D value of 0.48 cm^{-1}

from the $E_{\text{a}} = DS^2$ relationship is in agreement with the values obtained from the magnetization experiments.

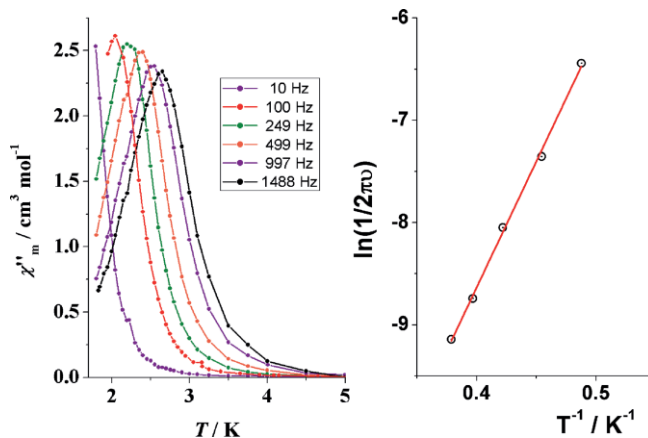


Figure 9. Left: out-of-phase peaks for (*S*)-**3** under a 0.1 T field at the indicated frequencies. Right: Arrhenius plot.

Among other factors, a parallel alignment of the easy axis of the Mn^{III} cations contributes to the enhanced global anisotropy of the system and the SMM response. Low-temperature studies (0.04–2 K) of ferromagnetic tetranuclear [Mn₄(sae)₄Cl₄] rings, which show a quasiperpendicular easy axes, revealed a weak anisotropy and energy barriers of ca. 5 cm^{-1} . The triangular systems derived from Schiff bases with one μ_3 -O ligand displaced from the Mn₃ plane are scarce,^[19] and an $S = 6$ ground state has been reported for only one of them.^[19b] As in the above case, the easy axes of the Mn^{III} cations are roughly perpendicular, the ground state was weakly anisotropic, and no SMM response was observed. In contrast, the easy axes for (*R*)-**3** and (*S*)-**3** are directed towards the μ_3 -Cl ligand and form a mean angle close to 65° , which allows a moderate total anisotropy and an appreciable E_{a} barrier.

Conclusions

The employment of enantiomerically pure Schiff bases is an excellent method to produce chiral clusters and chiral SMMs. The reported systems are the first polynuclear derivatives of the employed ligands, and a discrete triangular arrangement of Mn^{III} cations linked by one μ_3 -Cl bridge was isolated for the first time and gives unambiguous evidence of its ferromagnetic response. Complexes **3** exhibit the largest energy barriers for this family of clusters. Electronic circular dichroism is a fundamental tool for the full characterization of these kind of compounds, and a comparison between the solid and solution spectra provided information about the stabilities of the complexes in different media.

Experimental Section

Materials and Methods: The IR spectra ($\tilde{\nu} = 4000\text{--}400 \text{ cm}^{-1}$) were recorded with a Bruker IFS-125 FTIR spectrometer with samples prepared as KBr pellets. Variable-temperature magnetic studies were

performed with a Quantum Design MPMS-5 magnetometer operating at 0.03 T in the 300–2.0 K range. Diamagnetic corrections were applied to the observed paramagnetic susceptibilities by using Pascal's constants. The analysis of the magnetic data was performed with the PHI program.^[20] The qualities of the fits were parametrized by the value of $R = (\chi_M T_{\text{exp}} - \chi_M T_{\text{calcd.}})^2 / (\chi_M T_{\text{exp}})^2$.

The ECD and UV/Vis spectra were recorded with a Jasco J-715 spectrometer at room temperature with samples in spectroscopy-grade acetonitrile. Solutions in the concentration range $2.0\text{--}2.7 \times 10^{-4}$ mol dm⁻³ (i.e., 1.33–1.50 mg of sample per 5 mL of acetonitrile) were measured in three quartz cells with pathlengths of 2 cm ($\lambda = 850\text{--}450$ nm), 1 cm ($\lambda = 450\text{--}315$ nm), and 0.1 cm ($\lambda = 315\text{--}200$ nm). In each case, a tiny amount of the sample would not dissolve. All spectra were recorded at a scanning speed of 100 nm min⁻¹, a step size of 0.1 nm, a bandwidth of 2 nm, a response time of 0.5 s, and averaged over four accumulations. The baselines of the spectra were corrected with the solvent (acetonitrile) spectrum recorded under the same conditions immediately before or after the sample measurement. The ECD spectra were normalized to the UV/Vis spectra. The solid-state ECD spectra were obtained by placing a pellet in a rotating holder as close as possible to the photomultiplier tube of a Jasco J-715 spectrometer. Freshly prepared pellets with KCl as a matrix were measured in the range $\lambda = 240\text{--}800$ nm. In all cases, it was not possible to obtain a good quality spectrum below $\lambda = 270$ nm. The following measurement parameters were applied: scanning speed 100 nm min⁻¹, step size 0.1 nm, bandwidth 2 nm, response time 0.5 s, and four scans. The backgrounds of the resulting spectra were corrected. In each case, several spectra were obtained for one pellet, for which the disk was rotated around the incident axis direction and then flipped. The spectra were very similar, and no major differences were observed on the variation of rotation angle; therefore, the absence of spectral artefacts from linear dichroism and birefringence was confirmed.

Single-Crystal X-ray Crystallography: Prismlike specimens of the *R* and *S* enantiomers of **1–3** were used for the X-ray crystallographic analysis. The X-ray intensity data were measured with a Bruker D8-Venture system equipped with a multilayer monochromator and a Mo microfocus source ($\lambda = 0.71073$ Å). The frames were integrated with the Bruker SAINT software package with a narrow-frame algorithm. The final cell constants were based upon the refinement of the xyz centroids of reflections above $20\sigma(I)$. The data were corrected for absorption effects by the multiscan method (SADABS). The structures were solved with the Bruker SHELXTL software package and refined with SHELXL.^[21] Details of the crystal data, collection, and refinement for the pairs of enantiomers **1–3** are summarized in Table S1. The analyses of the structures and the preparation of the plots for publication were performed with the Ortep3^[22] and POVray programs.

The quality of the structure for (*S*)-**3** was below the quality standard for publication; thus, the complete structural data are not included in the work but unambiguous characterization was provided by the cell parameters and space group (Table S1), which agree with those obtained for (*R*)-**3**, and the partial data of the cluster confirms an identical structure.

CCDC 1492960 [for (*R*)-**1**], 1492961 [for (*S*)-**1**], 1492962 [for (*R*)-**2**], 1492963 [for (*S*)-**2**], 1492964 [for (*R*)-**3**], and 1492965 [for (*S*)-**3**] contain the supplementary crystallographic data for this paper. These data can be obtained free of charge from The Cambridge Crystallographic Data Centre.

Synthetic Procedures: Mn(PhCOO)₂ was synthesized in high yield (>80 %) by mixing stoichiometric amounts of aqueous solutions of

Na(PhCOO) and Mn(NO₃)₂. Mn(PhCOO)₂ precipitated immediately as a white powder, which was washed with cold water to remove soluble ions and air-dried. (*R*)- and (*S*)-2-phenylglycine and (*R*) and (*S*)-phenylalanine were purchased from TCI chemicals and used without further purification. Each pair of enantiomers was prepared by the same procedure; thus common syntheses will be described. The yields for **1–3** were ca. 25 %, and well-formed crystals were obtained and employed for instrumental measurements. The samples for analysis were dried gently to remove volatile solvents.

H₂L1 and H₂L2 Schiff Bases: Equimolar amounts of (*R*)- or (*S*)-2-phenylglycine (for H₂L1) or phenylalanine (for H₂L2) and salicylaldehyde were mixed in ethanol, and the mixture was heated under reflux for 1 h. The ligands were collected as yellowish solids in high yields after the concentration of the mother solutions.

[Mn₃(L1)₂(PhCOO)₄(MeOH)]·MeOH [(*R*)-1**-MeOH and (*S*)-**1**-MeOH]:** Mn(PhCOO)₂ (0.5 mmol, 0.167 g) and (*R*)- or (*S*)-H₂L1 (0.5 mmol, 0.121 g) were mixed in MeOH/MeCN (1:1), and the mixture was stirred for 1 h at room temperature. The resulting dark brown solution was filtered and left to diffuse slowly with Et₂O. Dark brown crystals suitable for XRD appeared after 24 h. C₅₈H₄₆Mn₃N₂O₁₂: calcd. C 61.77, H 4.11, N 2.48; found [(*R*)-**1**]/(*S*)-**1**] C 60.9/61.3, H 4.2/4.0, N 2.3/2.3. IR: $\tilde{\nu} = 3423.67$ (br), 2925.21 (br), 1598.48 (s), 1565.85 (s), 1538.66 (m), 1445.84 (w), 1395.35 (s), 1338.50 (m), 1287.31 (m), 1201.53 (w), 1147.38 (w), 1023.48 (m), 865.77 (s), 724.00 (m), 704.36 (w), 675.43 (w), 630.21 (w), 584.37 (w), 549.39 (m), 452.23 (w) cm⁻¹.

[Mn₃(L2)₂(PhCOO)₄]·Solvent [(*R*)-2**-5H₂O, (*S*)-**2**-2MeCN·MeOH-1.5H₂O]:** Mn(PhCOO)₂ (0.5 mmol, 0.167 g) and (*R*)- or (*S*)-H₂L2 (0.5 mmol) were mixed in MeOH/MeCN (1:1), and the mixture was stirred for 1 h at room temperature. The resulting solution was filtered and left to evaporate slowly. Dark brown crystals appeared after 24 h. C₆₁H₅₄Mn₃N₂O₁₃: calcd. C 61.68, H 4.58, N 2.36; found [(*R*)-**2**]/(*S*)-**2**] C 62.0/61.5, H 4.3/4.4, N 2.3/2.5. IR: $\tilde{\nu} = 3434.23$ (br), 3059.21 (w), 2930.64 (w), 1598.78 (s), 1569.96 (s), 1540.78 (s), 1491.65 (w), 1469.41 (w), 1446.43 (s), 1374.50 (s), 1299.23 (m), 1149.83 (w), 1051.26 (w), 1023.34 (w), 764.13 (w), 754.62 (w), 721.38 (m), 672.72 (w), 577.72 (m), 453.71 (w) cm⁻¹.

(Phgly)[Mn₃(L1)₃(μ₃-Cl)(Cl)₃]·Solvent [(*R*)-3**-0.5MeCN-0.25MeOH-0.5H₂O, (*S*)-**3**-0.5MeCN-0.5H₂O]:** MnCl₂·4H₂O (0.5 mmol, 0.197 g), (*R*)- or (*S*)-H₂L1 (0.5 mmol, 0.121 g), and Na(PhCOO) (0.5 mmol, 0.036 g) were dissolved in MeCN (20 mL), and the mixture was heated under reflux for 30 min. The solution was filtered and left to evaporate slowly. Dark brown crystals suitable for XRD appeared after two weeks.

The same product was obtained from an attempt to introduce an azide ion into the cluster with Na(PhCOO) replaced with NaN₃ (0.5 mmol, 0.033 g). C₅₃H₅₁Cl₄Mn₃N₄O₇: calcd. C 54.75, H 4.42, N 4.81; found [(*R*)-**3**]/(*S*)-**3**] C 55.1/55.4, H 4.1/4.5, N 4.9/4.6. IR: $\tilde{\nu} = 3446.7$ (br), 2926.72 (br), 1607.85 (s), 1541093 (m), 1492.22(w), 1441.13 (m), 1384.07 (w), 1293.49 (m), 1149.25 (w), 981.56 (w), 757.49 (m), 703.00 (m), 643.11 (w), 591.05 (m), 553.57 (s) cm⁻¹.

Supporting Information (see footnote on the first page of this article): Structural and ECD data.

Acknowledgments

Funding from the Ministerio de Economía y Competitividad, Project CTQ2015-63614-P, is acknowledged. M. G. thanks the Polish Ministry of Science and Higher Education ("Mobilność Plus" grant no. 1286/MOB/IV/2015/0) for support.

Keywords: Manganese · Schiff bases · Single-molecule magnets · Chirality · Cluster compounds

- [1] a) D. N. Woodruff, R. E. P. Winpenny, R. A. Layfield, *Chem. Rev.* **2013**, *113*, 5110–5148; b) J. D. Rinehart, J. R. Long, *Chem. Sci.* **2011**, *2*, 2078–2085; c) L. Ungur, S.-Y. Lin, J. Tang, L. F. Chibotaru, *Chem. Soc. Rev.* **2014**, *43*, 6894–6905.
- [2] a) K. Griffiths, C. W. D. Gallop, A. Abdul-Sada, A. Vargas, O. Navarro, G. E. Kostakis, *Chem. Eur. J.* **2015**, *21*, 6358–6361; b) G. Maayan, G. Christou, *Inorg. Chem.* **2011**, *50*, 7015–7021; c) N. C. Anastasiadis, D. A. Kalofolias, A. Philippidis, S. Tzani, C. P. Raptopoulou, V. Psycharis, C. J. Milios, A. Escuer, S. P. Perlepes, *Dalton Trans.* **2015**, *44*, 10200–10209.
- [3] J.-C. G. Bünzli, S. V. Eliseeva, *Chem. Sci.* **2013**, *4*, 1939–1949.
- [4] J.-C. G. Bünzli, S. V. Eliseeva, *Chem. Soc. Rev.* **2010**, *39*, 189–227.
- [5] a) S. Muhlbauer, B. Binz, F. Jonietz, C. Pfeleiderer, A. Rosch, A. Neubauer, R. Georgii, P. Boni, *Science* **2009**, *323*, 915–919; b) X. Z. Yu, Y. Onose, N. Kanazawa, J. H. Park, J. H. Han, N. Nagaosa, Y. Tokura, *Nature* **2010**, *465*, 901–904.
- [6] a) J. Kishine, K. Inoue, Y. Yoshida, *Prog. Theor. Phys. Suppl.* **2005**, *159*, 82–95; b) Y. Togawa, T. Koyama, K. Takayanagi, S. Mori, Y. Kousaka, J. Akimitsu, S. Nishihara, K. Inoue, A. S. Ovchinnikov, J. Kishine, *Phys. Rev. Lett.* **2012**, *108*, 107202.
- [7] a) H. Asada, M. Ozeki, M. Fujiwara, T. Matsushita, *Chem. Lett.* **1999**, *28*, 525–526; b) H. Asada, M. Ozeki, M. Fujiwara, T. Matsushita, *Polyhedron* **2002**, *21*, 1139–1148; c) M. Dey, C. P. Rao, P. K. Saarenketo, K. Rissanen, E. Kolehmainen, P. Guionneau, *Polyhedron* **2003**, *22*, 3515–3521; d) C. P. Pradeep, T. Htwe, P. S. Zacharias, S. K. Das, *New J. Chem.* **2004**, *28*, 735–739; e) C. P. Pradeep, P. S. Zacharias, S. K. Das, *Polyhedron* **2005**, *24*, 1410–1416; f) C. P. Pradeep, P. S. Zacharias, S. K. Das, *J. Chem. Sci.* **2006**, *118*, 311–317; g) S.-Z. Zhan, Y.-J. Zhang, J.-G. Wang, *Acta Crystallogr., Sect. E: Struct. Rep. Online* **2006**, *62*, m2713–m2714; h) C. P. Pradeep, P. S. Zacharias, S. K. Das, *Inorg. Chem. Commun.* **2008**, *11*, 89–93.
- [8] R. Inglis, F. White, S. Piligkos, W. Wernsdorfer, E. K. Brechin, G. S. Papaefstathiou, *Chem. Commun.* **2011**, *47*, 3090–3092.
- [9] a) Y.-Y. Zhu, C. Cui, Y.-Q. Zhang, J.-H. Jia, X. Guo, C. Gao, K. Qian, S.-D. Jiang, B.-W. Wang, Z.-M. Wang, S. Gao, *Chem. Sci.* **2013**, *4*, 1802–1806; b) Y.-Y. Zhu, C. Cui, K. Qian, J. Yin, B.-W. Wang, Z.-M. Wang, S. Gao, *Dalton Trans.* **2014**, *43*, 11897–11907.
- [10] L.-F. Zhang, Z.-H. Ni, Z.-M. Zong, X.-Y. Wei, C.-H. Ge, H.-Z. Kou, *Acta Crystallogr., Sect. C: Cryst. Struct. Commun.* **2005**, *61*, m542–m544.
- [11] a) Y.-G. Li, L. Lecren, W. Wernsdorfer, R. Clerac, *Inorg. Chem. Commun.* **2004**, *7*, 1281–1284; b) H.-C. Yao, M.-M. Li, L.-M. Zheng, Z.-J. Li, *J. Coord. Chem.* **2008**, *61*, 2814–2822.
- [12] a) C. Boskovic, E. Rusanov, H. Stoeckli-Evans, H. U. Gudel, *Inorg. Chem. Commun.* **2002**, *5*, 881–886; b) C. Boskovic, R. Bircher, P. L. W. Tregenna-Piggott, H. U. Gudel, C. Paulsen, W. Wernsdorfer, A.-L. Barra, E. Khatsko, A. Neels, H. Stoeckli-Evans, *J. Am. Chem. Soc.* **2003**, *125*, 14046–14058; c) S. Nayak, G. Novitchi, S. Muche, D. Luneau, S. Dehnen, *Z. Anorg. Allg. Chem.* **2012**, *638*, 1127–1133.
- [13] Y.-G. Li, Q. Wu, L. Lecren, R. Clerac, *J. Mol. Struct.* **2008**, *890*, 339–345.
- [14] N. Hoshino, T. Ito, M. Nihei, H. Oshio, *Inorg. Chem. Commun.* **2003**, *6*, 377–380.
- [15] a) Q. Wu, Q. Shi, Y.-G. Li, E.-B. Wang, *J. Coord. Chem.* **2008**, *61*, 3080–3091; b) Y. Ding, J. Xu, Z. Pan, H. Zhou, X. Lou, *Inorg. Chem. Commun.* **2012**, *22*, 40–43.
- [16] a) Q. Li, J. B. Vincent, E. Libby, H.-R. Chang, J. C. Huffman, P. D. W. Boyd, G. Christou, D. N. Hendrickson, *Angew. Chem. Int. Ed. Engl.* **1988**, *27*, 1731–1733; *Angew. Chem.* **1988**, *100*, 1799; b) S. Wang, K. Folting, W. E. Streib, E. A. Schmitt, J. K. McCusker, D. N. Hendrickson, G. Christou, *Angew. Chem. Int. Ed. Engl.* **1991**, *30*, 305–306; *Angew. Chem.* **1991**, *103*, 314; c) D. N. Hendrickson, G. Christou, E. A. Schmitt, E. Libby, J. S. Bashkin, S. Wang, H.-L. Tsai, J. B. Vincent, P. D. W. Boyd, J. C. Huffman, K. Folting, Q. Li, W. E. Streib, *J. Am. Chem. Soc.* **1992**, *114*, 2455–2471; d) M. W. Wemple, H.-L. Tsai, K. Folting, D. N. Hendrickson, G. Christou, *Inorg. Chem.* **1993**, *32*, 2025–2031; e) S. Wang, H.-L. Tsai, E. Libby, K. Folting, W. E. Streib, D. N. Hendrickson, G. Christou, *Inorg. Chem.* **1996**, *35*, 7578–7589.
- [17] T. Wu, X.-Z. You, P. Bouř, *Coord. Chem. Rev.* **2015**, *284*, 1–18.
- [18] a) A. Ipatov, F. Cordova, L. J. Doriol, M. E. Casida, *J. Mol. Struct.* **2009**, *914*, 60–73; b) M. Enamullah, M. A. Quddus, M. R. Hasan, G. Pescitelli, R. Berardozi, G. Makhlofi, V. Vasylyeva, Ch. Janiak, *Dalton Trans.* **2016**, *45*, 667–680.
- [19] a) M. Nihei, N. Hoshino, T. Ito, H. Oshio, *Chem. Lett.* **2002**, *31*, 1016–1017; b) P. Chaudhuri, R. Wagner, T. Weyhermuller, *Eur. J. Inorg. Chem.* **2010**, 1339–1342; c) C.-M. Liu, D.-Q. Zhang, D.-B. Zhu, *Dalton Trans.* **2010**, *39*, 1781–1785.
- [20] N. F. Chilton, R. P. Anderson, L. D. Turner, A. Soncini, K. S. Murray, *J. Comput. Chem.* **2013**, *34*, 1164–1175.
- [21] G. M. Sheldrick, *Acta Crystallogr., Sect. A: Fundam. Crystallogr.* **2008**, *64*, 112–122.
- [22] Ortep-3 for Windows: L. J. Farrugia, *J. Appl. Crystallogr.* **1997**, *30*, 565.

Received: September 15, 2016

Published Online: ■

Chiral Magnets

A. Escuer,* J. Mayans,
M. Font-Bardia, L. Di Bari,
M. Górecki 1–9



**Trinuclear Complexes Derived from
R/S Schiff Bases – Chiral Single-Mol-
ecule Magnets**



The employment of enantiomerically pure Schiff bases allows the synthesis of the *R* and *S* pairs of trinuclear chiral clusters. Two discrete triangular Mn^{III}_3 enantiomers with one $\mu_3\text{-Cl}$ bridge exhibit single-molecule magnet (SMM) responses.

DOI: 10.1002/ejic.201601138